Impacts of Soft Robotic Actuator Geometry on End Effector Force and Displacement

Moaed A. Abd, Craig Ades, Mohammad Shuqir, Mohammed Holdar, Mostapha Al-Saidi,

Nicholas Lopez and Erik D. Engeberg

Ocean &Mechanical Engineering Department

College of Engineering and Computer Science.

Florida Atlantic University.

mabd2015@fau.edu, cades@my.fau.edu, mshuqir2016@fau.edu, mholdar2016@fau.edu, malsaidi2015@fau.edu, nlopez2015@fau.edu, eengeberg@fau.edu

ABSTRACT

Soft Pneumatic Actuators (SPA's) received a great interest in the recent years, due to their flexibility and inherent safety with everyday users. SPA's are primarily composed of easily deformable non-rigid materials such as fluids, gels, and elastomers. This study focuses on how varying taper angle parameter (θ) impacts the performance of the soft robotic actuator, specifically, the width of the SPA decreased toward the tip with a trapezoidal footprint. The study includes 7 models with taper angle θ varying from 0^0 to 6^0 with 1^0 increments, all other geometric parameters were constant. The actuators were tested with frequencies from 1 to 6 rad/s, then the actuators were tested at the frequency of 0.5 rad/s to obtain the maximum force. It was found that highest force applied by the tip of the soft actuator occurs with taper angle of 2^0, whereas the maximum displacement of the tip of the actuator was achieved with a taper angle of 6^0.

Keywords

Soft actuator, Soft Robot, Pneumatic actuator.

1. INTRODUCTION

Recent developments in robotic technology have shifted from rigid mechanisms based on gears-bearings-motors to a softer biologically inspired actuator [1]. One prime advantage of soft robotics is the ability to interact with soft and delicate objects.

Conventional robots are designed to do manufacturing tasks like the ones used in the food and automotive industries. They are less safe to interact with a human being or any biological system due to its rigidity. Conventional robots have difficulty manipulating delicate objects without harming them. This issue can be mitigated by using soft actuators [2], [3].

The developing field of soft robotics holds great potential for bringing robots into all aspects our daily lives, especially areas previously prohibitive for rigid robots. Soft actuators are becoming an essential part of the robotics community, the reason is that it provides a solution for many challenges that conventional robotics faces [4], for instance, uncertainty about the orientation and the shape of the objects that the robot intended to move [5].

Soft robotics can gently interact with the surrounding environment which makes it more reliable to deal with any delicate objects [6],[7]. SPAs function via pressurized fluid flow through a common channel that inflates flexible chambers to achieve bending motion. The angular speed of bending of a structure actuated by a pneunet depends upon: i) the rate of inflation, ii) the geometry of the internal channels and exterior walls, and iii) the properties of the structure [16]. Pneumatic actuation was used, since pressurized air has four advantages: i) it provides rapid inflation of the pneumatic structure; ii) it is easily controlled and measured; iii) it is almost universally available; iv) it is light in weight; v) it can be discarded after use by venting to the atmosphere [16].

Several prior applications of soft robotics includes wearable robotics [8], medical robots [9], and micromanipulation [10]. Soft robotics application in the medical field, for example, Harvard Biodesign Lab is using soft robotics to help patients who have had heart failure [11]. For manipulating small and delicate items, soft grippers and control systems have been made for pick and place tasks with high-speed precision for handling fresh eggs. Mimicry of swimming underwater biological system seen in nature have been demonstrated by the Jennifish in the BioRobotics Lab at FAU [12], among applications demonstrated by other researchers such as robotic octopuses and peristaltic robots [13], [14], [15].

Since soft robotics is an emerging field, there is a need to study different parameters and its effects on the applied force, end effector position and velocity. In this paper, the design, fabrication, and evaluation of seven soft actuators will be described. The taper angle θ was the only geometric parameter that was varied among the seven actuators to determine the impact that a narrowing, trapezoidal form factor had upon actuator force and displacement.

2. METHODOLOGY

The purpose of this study is to investigate the impact that soft actuator taper angle has upon the force and displacement of the actuator. When changing the taper angle, the actuator size changes and the chamber size narrows along the length of the actuator so it is expected that the performance will change.

Seven SPAs, each with a different taper angle ranging from 0° to 6° in 1° increments were designed in this paper, while the other parameters were constant.

2.1 Designing the actuators

SolidWorks 2015 was used to modify the molds to create actuators conceptualized in [17]. For consistency among the seven actuators designed in this paper, an inlet nozzle was added to the main design to make sure that the inlet fluid had the same connection (Figure 1). Three different mold parts were designed to manufacture the actuator. The Bottom part is used to make the cavity of chambers; the top part is used to separate the chambers and the base part was used to unify the top and bottom of the actuator. Mold parts for ($\theta = 3^0$) are shown in Figure 1.

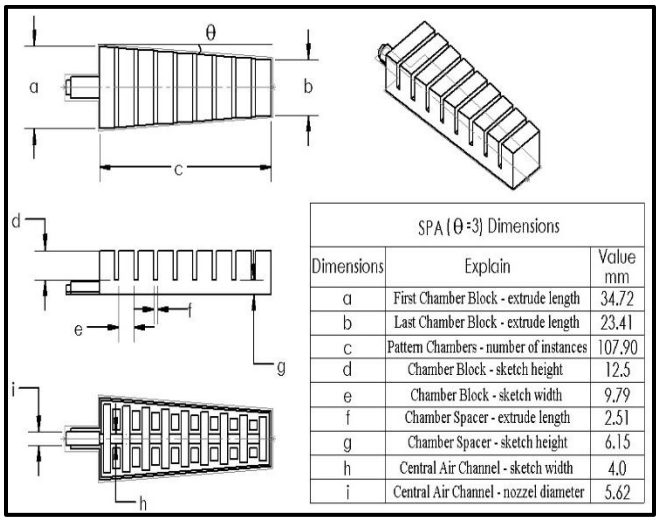

SPA (θ=3) Dimensions

Dimensions	Explain	Value mm
a	First Chamber Block - extrude length	34.72
b	Last Chamber Block - extrude length	23.41
c	Pattern Chambers - number of instances	107.90
d	Chamber Block - sketch height	12.5
e	Chamber Block - sketch width	9.79
f	Chamber Spacer - extrude length	2.51
g	Chamber Spacer - sketch height	6.15
h	Central Air Channel - sketch width	4.0
i	Central Air Channel - nozzel diameter	5.62

Figure 1. Soft Actuator Dimensions for $\theta = 3^0$.

2.2 3D Printing Molds

The SolidWorks models for the molds were 3D printed. Ultimaker3 (Ultimaker, Netherlands) was used to print all the molds using PLA. The mold for SPA with taper angle θ=30 is shown in Figure 2.

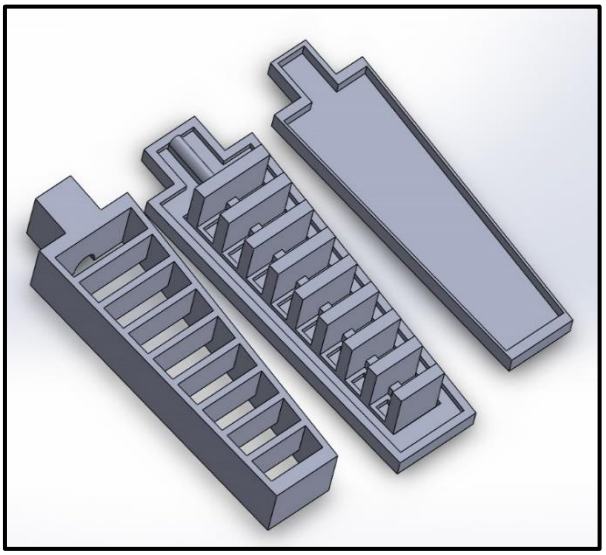

Figure 2. SolidWorks Design mold for $\theta = 3^0$.

2.3 Molds Fabrication

After finishing the 3D printing, the top and bottom parts were put together to hold the Ecoflex 00-30 (Smooth-On, Inc. Macungie, PA, USA). Ecoflex 00-30 has a Young's modulus ~ 0.1 Mpa, and a Shore hardness of 30, and is the material that was used in fabrication the soft actuators. Hot glue was applied to bind the top and bottom molds together to keep the material from leaking. Before pouring the Ecoflex 00-30, Easy Release (Smooth-On, Inc. Macungie, PA, USA) was used to ease removing the actuator from the mold. Figure 3 Shows the fabricated soft actuators.

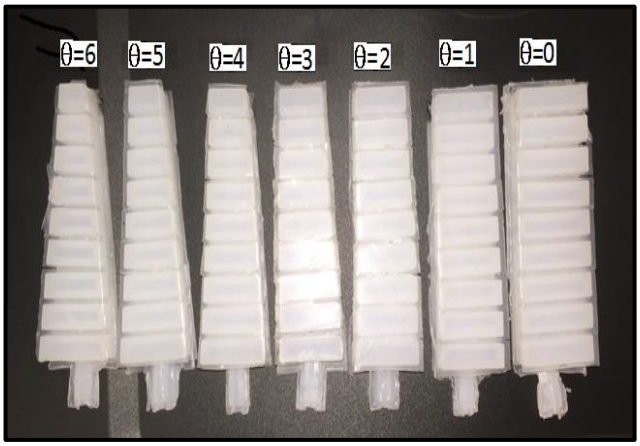

Figure 3. Fabricated Soft Actuators.

3. EXPERIMENT SETUP AND DATA ACQUISITION

3.1 Testing Station

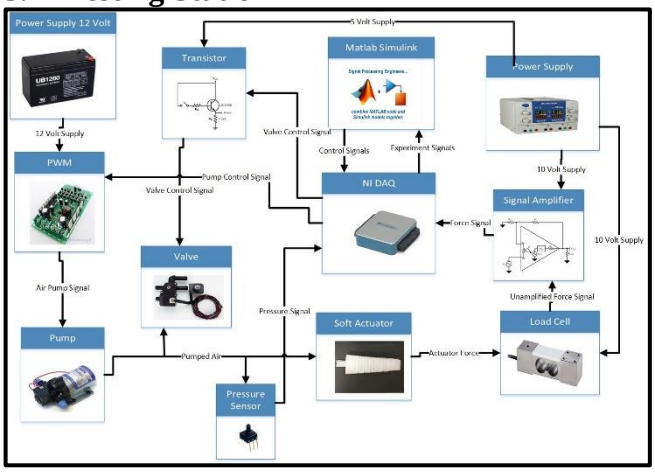

Figure 4. Hardware configuration of Testing station

The testing station (Figure 4) consists of a mount for the actuator, a 1kg load cell (LSP-1 from Transducer Techniques) to record the applied force at the tip of the actuator, a 12V 2-way solenoid valve to direct air flow, a 0-15psi pressure sensor from Honeywell to measure pump pressure, a motor driver (Syren 50A) to drive the air pump and a National Instruments DAQ to integrate all components into the computer for control from Matlab/Simulink.

3.2 Controller

The controller was designed using Simulink (Figure 5). It is an open loop controller that uses a sine wave input to control the on/off for the air pump, the open/close of the solenoid valve, and to measure the pressure of the air pump and the force applied to the load cell by the actuator. Whenever the sine wave is positive the valve is closed and the pump is simultaneously turned on to inflate the actuator.

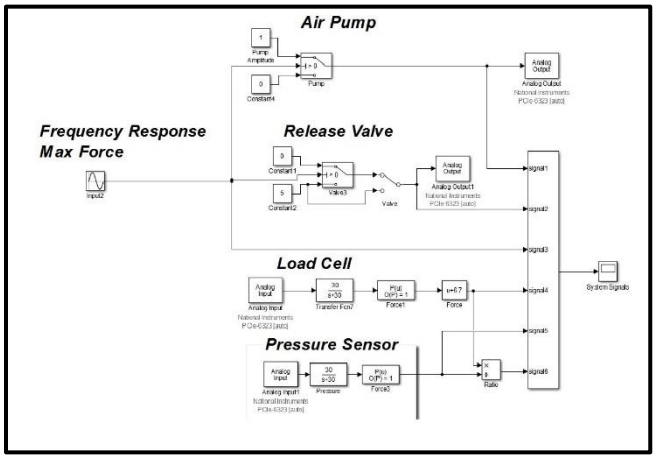

Figure 5. Matlab Simulink controller

Conversely, negative sine wave signals cause the pump to turn off and the valve to open, deflating the actuator. This illustrates the method of inflation/deflation that causes the actuator to apply force to the load cell.

3.3 Calibration

Once the system was assembled the load cell needed to be calibrated. This was achieved by incrementally placing known mass onto the load cell and recording the corresponding output voltage from the load cell. Microsoft Excel provided a linear equation relating the voltage to the applied load with a correlation coefficient of 1.

3.4 Force Measurement Procedure

To gather the data for the experiment the actuator was inflated/deflated twenty times at six different frequencies ranging from 1 to 6 rad/s incremented by 1 rad/s. First, the inflation tube was inserted into the actuator and a zip-tie used to secure it in place. The tip of the actuator was then aligned to a mark on the load cell. The power was turned on and the battery plugged in. Finally, the actuators were tested at a lower frequency of 0.5 rad/sec to find the maximum applied load. For each frequency, the actuator was run for 20 cycles.

3.5 Motion Tracking

The actuator was then rotated to enable unconstrained motion and a black dot was marked on the tip. A GoPro HERO 5 was used to record the motion of the actuator when it was inflated to its unrestricted maximum flexion range and then deflated. Care was taken to ensure that the motion of the actuator was planar, in the field of view of the camera. KINOVEA was used to track the planar motion of the black mark on the tips of the actuators. The x-y planar displacement was output to an excel spreadsheet. Figure 6 shows a photo sequence of the actuator during motion.

3.6 Analysis

Upon completion of gathering all the data, analyses were performed to obtain plots of force vs. time, force/pressure vs. time, force vs. pressure, the paths of the tips of the actuators, and the mean and standard deviation of the maximum forces for each frequency. Also, a 1-way ANOVA was performed to test the impact that actuation frequency had upon the force generated.

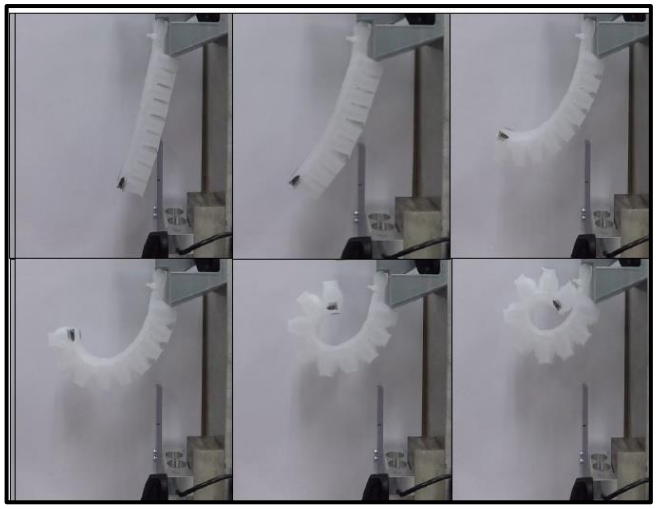

Figure 6. KINOVEA Photo Sequences

4. RESULTS AND DISCUSSION

Figure 7, shows the Force with respect to time for an actuator with taper angle 0°, for all seven frequencies respectively.

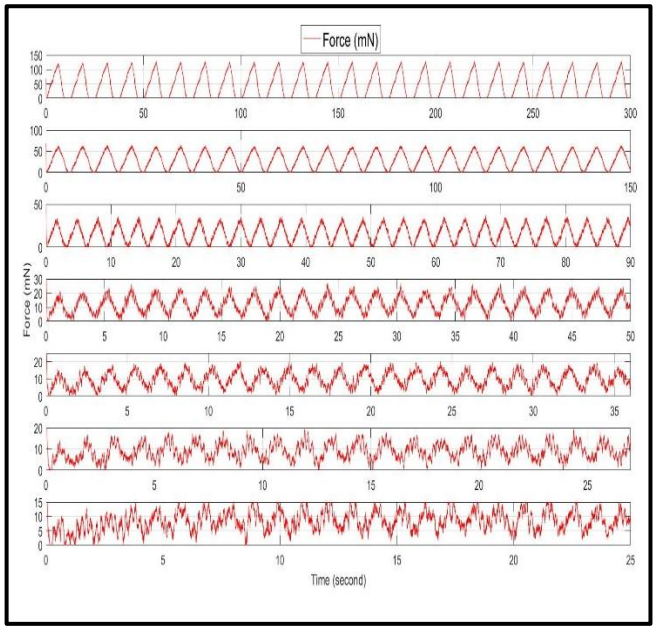

Figure 7. Force for a soft actuator with taper angle 0^0.

The graph shows that the maximum force occurs when the frequency is minimum (0.5 rad/s), in general as the frequency increased the force applied by the soft actuator decreased. This behavior was observed for all the soft actuators with different taper angles.

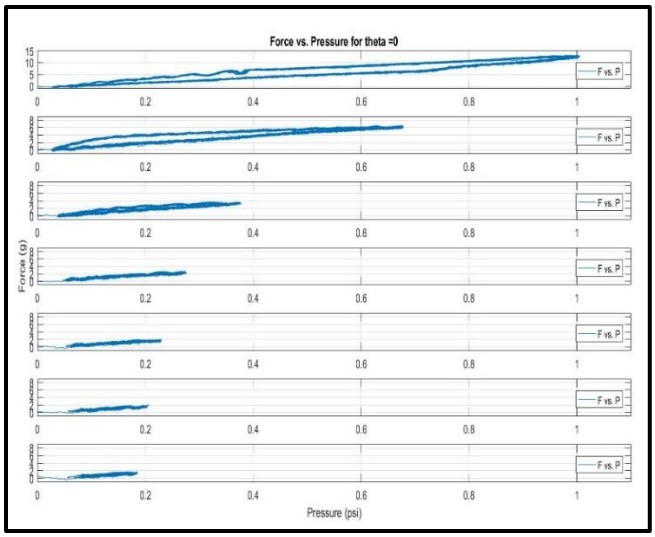

Figure 8. Hysteresis of the soft actuator with taper angle 0^0 for all frequencies.

Figure 8 shows a hysteresis loop; the energy losses are maximum when the frequency is minimum.

As the frequency increase the energy losses decreases, the reason is when the frequency is the minimum the actuation time is longer in comparison to a higher frequency, which means the energy provided to the system is higher.

The input energy to the system is the pressurised air, while the output is the force applied by the soft actuator. Figure 9 represents the Ratio of force over pressure, Force and Pump signal for all the actuators at maximum frequency (0.5 rad/s). When the pump turns on, the actuators started to inflate causing the actuator to apply the force at their tips. As the pressure built up in the actuators, the force increased gradually and reaches its maximum value. Then the pump signal turned off, causing the actuators to deflate, the sudden decrease in actuator pressure causes a high force to pressure ratio in some of the actuators, which explains the spikes of the ratio after the pump signal turns off.

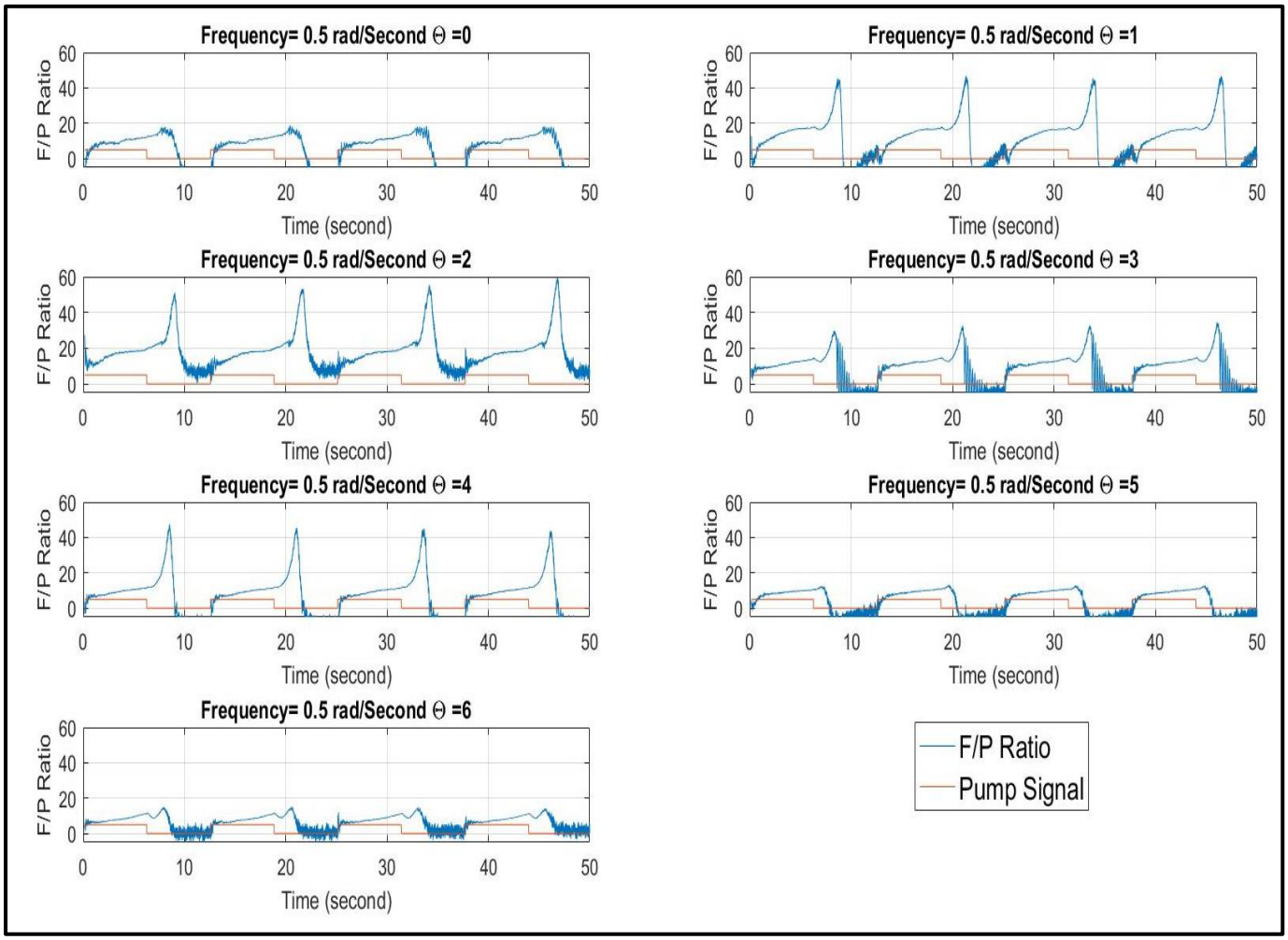

Figure 9. Force, Ratio of Force over Pressure and Pump signal for the tested actuators over maximum frequency (0.5 rad/s)

Figure 10 shows the displacement of the soft actuator's tips during inflation in the x-y plane with frequency 0.5 rad/s. The displacement increases as the taper angle increased, with a maximum displacement produced by the actuator with a taper angle 6°.

Figure 11 shows a comparison of Mean and standard deviation for maximum forces for all the soft actuators over different frequencies. In general, the mean of maximum force is at the lowest frequency as discussed previously for all actuators. The figure also shows how the mean Force changes when changing the taper angle. It can be noticed from the figure that the soft actuator with taper angle 2° has the best performance, as it has the largest mean maximum force over all the frequencies.

One-way analysis of variance (ANOVA1) was used to statistically analyze the mean of maximum force with different frequencies to find any correlation between the two of them for each soft actuator. The result of ANOVA1 shows that the actuation frequency significantly impacted the maximum force generated ($p<0.05$).

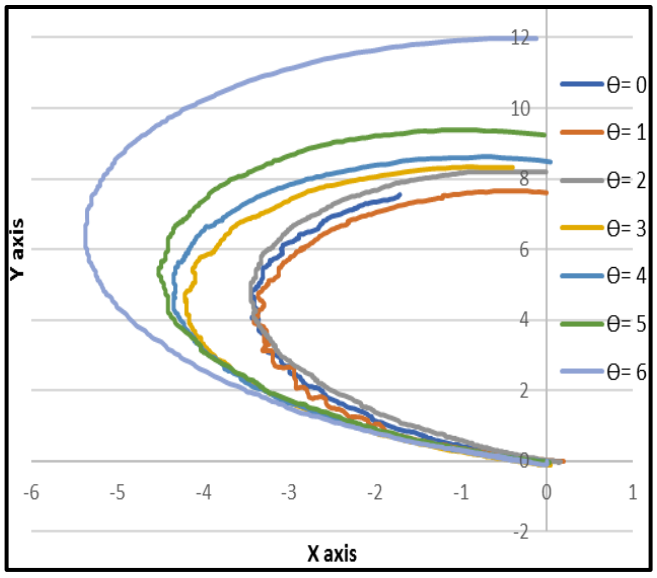

Figure 10. Displacement of the tip of the soft actuators

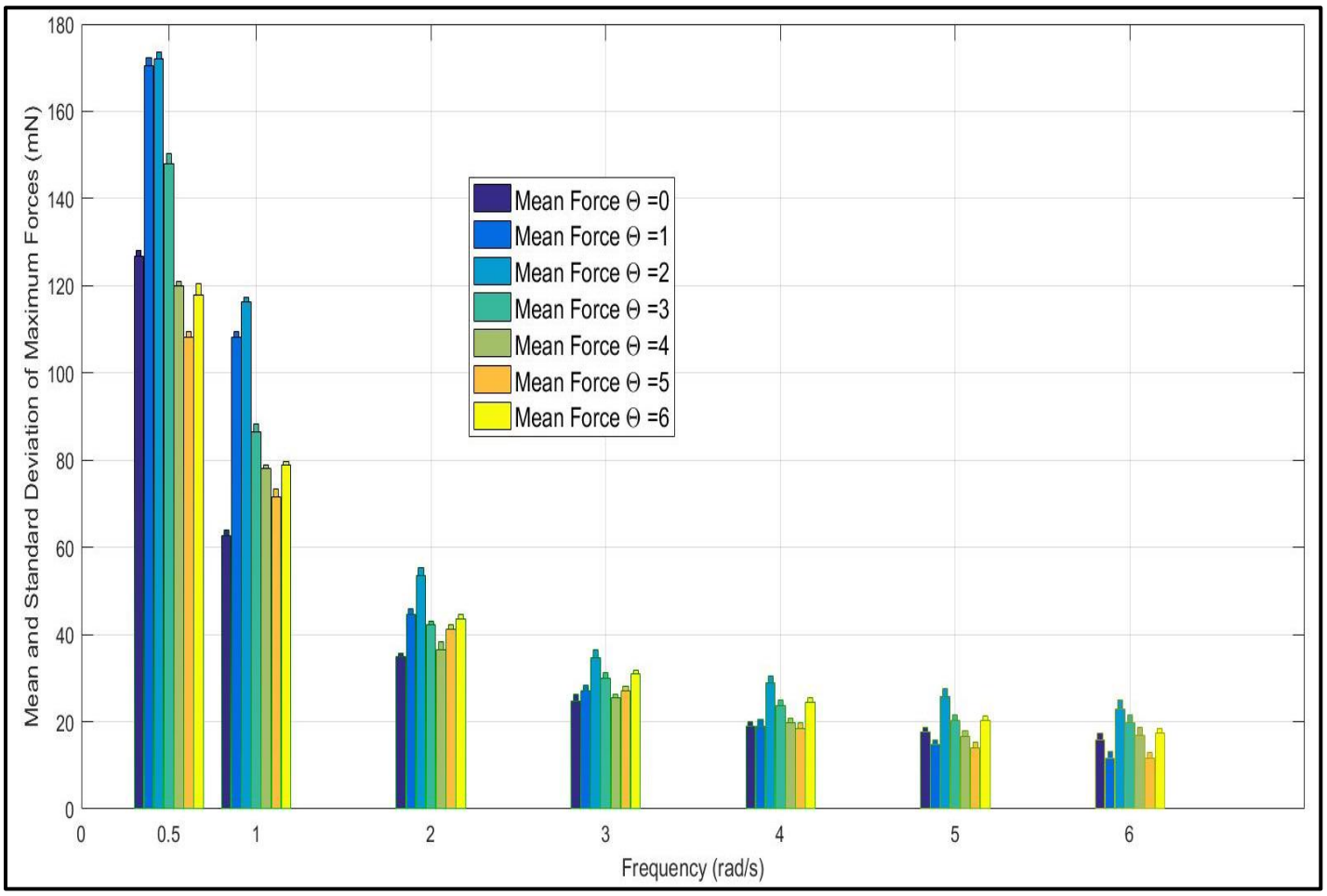

Figure 11. Standard deviation and mean of maximum forces for all the actuators at different frequencies

5. CONCLUSION

Seven different soft pneunet actuators were designed and evaluated in this paper. It has been shown in this study that changing the taper angle of the soft actuators affect the performance of the actuators in different ways. In our case, the force output by the actuator with a taper angle of 2° produced the largest force, whereas the actuator with a taper angle of 6° produced the most displacement in unconstrained tests. Also, it was noted that the actuation frequency significantly impacted the applied force with all seven actuators.

6. REFERENCES

[1] N. Tsagarakis and Darwin G. Caldwell. (2000). Improved Modelling and Assessment of pneumatic Muscle Actuators. IEEE International Conference on Robotics and Automation. 3641-3646.

[2] Homberg B, Katzschmann RK, Dogar M, Rus D. (2015). Haptic identification of objects using a modular soft robotic gripper. IEEE/RSJ International Conference on Intelligent Robots and Systems (IROS).

[3] E. Brown, N. Rodenberg, J. Amend, A. Mozeika, E. Steltz, M. R. Zakin, H. Lipson, and H. M. Jaeger. (2010). Universal robotic gripper based on the jamming of granular material. Proceedings of the National Academy of Sciences, vol. 107, no. 44, pp. 18 809–18 814.

[4] Haddadin, S., Albu-Schaffer, A. and Hirzinger, G. (2009). Requirements for Safe Robots: Measurements, Analysis and New Insights. The International Journal of Robotics Research, 28: 1507-1527.

[5] Doulgeri, Z. and Fasoulas, J. (2003). Grasping control of rolling manipulations with deformable fingertips. Mechatronics, IEEE/ASME Transactions on, 8(2), 283-286.

[6] R. K. Katzschmann, A. D. Marchese, and D. Rus. (2015). Autonomous object manipulation using a soft planar grasping manipulator. Soft Robot., vol. 2, no. 4, pp. 155–164.

[7] K. C. Galloway et al. (2016). Soft robotic grippers for biological sampling on deep reefs," Soft Robot., vol. 3, no. 1, pp. 23–33.

[8] P. Polygerinos, Z. Wang, K. C. Galloway, R. Wood, and C. J. Walsh. (2014). Soft robotic glove for combined assistance and at-home rehabilitation. Robot. Auton. Syst., vol. 73, pp. 135–143.

[9] T. Noritsugu and T. Tanaka. (2002). Application of rubber artificial muscle manipulator as a rehabilitation robot. IEEE/ASME Trans. on Mechatronics, vol. 2, no. 4, pp. 259–267.

[10] Ilievski, F., Mazzeo, A. D., Shepherd, R. F., Chen, X. and Whitesides, G. M. (2011). Soft Robotics for Chemists. Angew. Chem., 123: 1930–1935. doi: 10.1002/ange. 201006464.

[11] Soft Robotics. Harvard Biodesign. 2015. Accessed 10.29.2016. http://biodesign.seas.harvard.edu/soft-robotics

[12] Jennifer Frame, Oscar Curet and Erik D. Engeberg. (2016) Free-Swimming Soft Robotic Jellyfish. The 29th Florida Conference on Recent Advances in Robotics (FCRAR).

[13] Kim, S., Laschi, C. and Trimmer, B. (2013). Soft robotics: a bioinspired evolution in robotics. Trends in biotechnology, vol. 31, no. 5, pp. 287-294.

[14] C. Laschi, M. Cianchetti, B. Mazzolai, L. Margheri, M. Follador, and P. Dario. (2012). Soft robot arm inspired by the octopus. Adv. Robot., vol. 26, pp. 709–727.

[15] Chen, F. J., Dirven, S., Xu, W. L., and Li, X. N. (2014). Soft actuator mimicking human esophageal peristalsis for a swallowing robot. Mechatronics, IEEE/ASME Transactions on, 19(4), 1300-1308.

[16] Bobak Mosadegh , Panagiotis Polygerinos , Christoph Keplinger , Sophia Wennstedt , Robert F. Shepherd , Unmukt Gupta , Jongmin Shim , Katia Bertoldi , Conor J. Walsh , and George M. Whitesides. (2014). Pneumatic Networks for Soft Robotics that Actuate Rapidly. Advanced Functional Material, 24, 2163–2170.

[17] Soft Robotics Toolkit. Accessed 03.01.2017. http://softroboticstoolkit.com/book/pneunets-design.